Hydrodynamics and Mass Transfer in Gas-Liquid Flows in Microreactors

Pawel Sobieszuk, Joelle Aubin, Ryszard Pohorecki

Paweł Sobieszuk[1]
Joëlle Aubin[2]
Ryszard Pohorecki[1]

[1] Warsaw University of Technology, Faculty of Chemical and Process Engineering, Warsaw, Poland.

[2] Université de Toulouse, Laboratoire de Génie Chimique, Toulouse, France.

Review

Hydrodynamics and Mass Transfer in Gas-Liquid Flows in Microreactors

Over the last ten to fifteen years, microreaction technology has become of increased interest to both academics and industrialists for intensification of multiphase processes. Amongst the vast application possibilities, fast, highly exothermic and/or mass transfer-limited gas-liquid reactions benefit from process miniaturization. Recent studies of hydrodynamics and mass transfer in gas-liquid microreactors with closed and open microchannels, e.g., falling-film microreactors, are reviewed and compared. Special attention is paid to Taylor or slug flow in closed channels, as this regime seems to be most adapted for practical engineering applications.

Keywords: Gas-liquid reaction, Hydrodynamics, Mass transfer, Microchannel, Microreactor, Taylor flow

DOI: 10.1002/ceat.201100643

1 Introduction

The use of microreaction technology for applications in process industries has developed significantly over the last decade as a means of process intensification. Microreactors and microstructured process equipment offer high surface-to-volume ratios, short diffusion and conduction paths, high interfacial areas, and strictly controlled flow conditions which allow significant intensification of mass and heat transfer processes as well as inherently cleaner and safer chemical production. These features are particularly attractive for fast, highly exothermic (or endothermic) and/or mass transfer-limited reactions as well as high-temperature and -pressure processes occurring especially in multiphase (gas-liquid, liquid-liquid, gas-solid, liquid-solid, or gas-liquid-solid) systems [1, 97, 98]. Amongst the different applications of microreactors, a number of studies have demonstrated the potential of this type of technology for difficult and typically dangerous gas-liquid and gas-liquid-solid catalytic reactions, such as the direct synthesis of hydrogen peroxide [2], direct fluorination [3–5], three-phase hydrogenation reactions [6–9], and photochemical gas-liquid reactions [10]. In addition to the demonstrative studies on the potential application of gas-liquid microreactors, the literature involves now more fundamental investigations concerning the operation of these devices and their design. Much effort has been spent to understand the links between process parameters (equipment design and operating conditions) and the gas-liquid hydrodynamics as well as the intensification of mass and heat transfer. In recent years, a number of comprehensive review articles have appeared in the literature, dealing with various aspects of gas-liquid flows in microreactors including flow patterns [12], Taylor flow [11, 47, 96], and mass transfer [100].

This review focuses on comparing our data on gas-liquid hydrodynamics and mass transfer in microreactors with those presented in the literature and on suggesting possible directions for future work. The article is divided into two sections: open microchannels and closed microchannels. In microreactors and microstructured process equipment, open microchannels are grooves in a flat plate that are open on one side to ensure contact with the other phase. Closed microchannels are microtunnels of arbitrary cross-sectional shape through which both phases are contacted simultaneously. Closed microchannels are more commonly used in microreaction technology, and a large number of fundamental studies have been devoted to better understanding the flow structure and process intensification engendered by these devices. The first section on gas-liquid flows in closed microchannels concentrates particularly on Taylor flow, providing insight on bubble generation, liquid-phase hydrodynamics, pressure drop, and mass transfer. The second part on open microchannel devices deals with the gas-liquid hydrodynamics and mass transfer in falling-film microreactors.

Correspondence: Dr. P. Sobieszuk (sobieszuk@ichip.pw.edu.pl), Warsaw University of Technology, Faculty of Chemical and Process Engineering, Warynskiego 1, PL-00-645 Warsaw, Poland.

2 Closed-Channel Microreactors

2.1 Flow Regimes

The gas-liquid flow regime describes the spatial distribution of the two-phase flow in the microchannels and is important because it strongly influences the performance of the microreactor, particularly in terms of pressure drop, heat and mass transfer. A number of flow regimes can occur, which depend on several factors, including the gas and liquid flow rates, the fluid properties (e.g., surface tension, viscosity, density), the wettability of the microchannel wall by the liquid (i.e., contact angle) as well as the channel size and geometry (including the channel cross section and inlet geometry).

A large number of experimental studies presented in the literature have been dedicated to the study of flow regimes in small tubes and microchannels. An extensive review of these studies has been published by Shao et al. [12]. Five predominant flow regimes are typically observed: bubbly, Taylor, Taylor-annular, annular, and churn flow. Dispersed flow, which is commonly observed in macroscale tubes, is rarely observed in microchannels. Fig. 1 presents the flow regimes identified for air-water flow at different superficial gas and liquid velocities (U_{GS}, U_{LS}) in a 1-mm diameter circular tube [13]. Although the exact positions of the transition lines between flow regimes depend on the gas-liquid system studied, the arrangement and size of the regions of the different flow regimes are representative of a large number of systems.

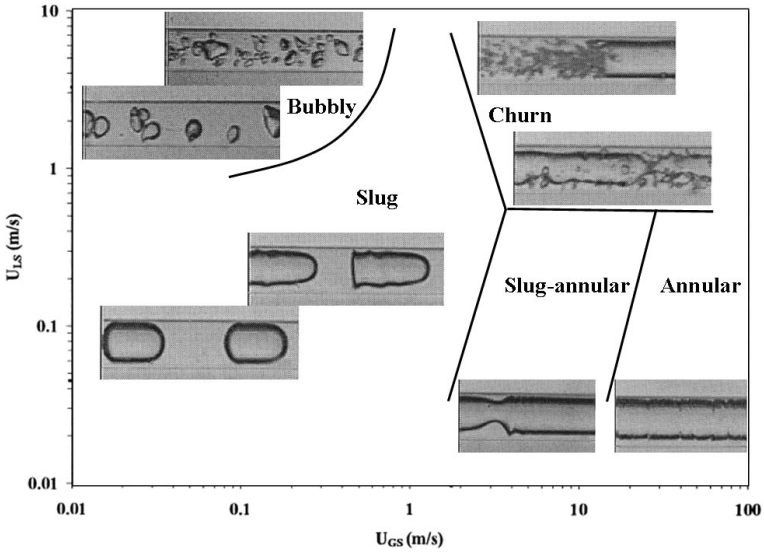

Figure 1. Example of a flow regime map for gas-liquid flow in microchannels. Adapted from [13].

The type of flow regime occurring in the microchannel strongly influences the performance of the operation being carried out in the reactor and it is therefore important to be able to predict the flow regime generated. Flow regime maps, like that shown in Fig. 1, depict the regions in which a given flow pattern occurs as a function of operating conditions, typically the superficial gas and liquid velocities. A number of flow regime maps for gas-liquid flow in microchannels have been proposed in the literature (e.g., [13–21]) for various channel sizes, cross sections (circular, triangular, square, and rectangular) and materials as well as fluid properties. Depending on these properties, the boundaries between the different flow regimes may be shifted to higher or lower superficial gas and liquid velocities. This can be seen, e.g., in Fig. 2, where the flow pattern map obtained by Sobieszuk et al. [16] in a 400-µm glass capillary for N_2-ethanol flow is compared with that obtained by Triplett et al. [13]. The data by Sobieszuk et al. [16] do not show the bubbly and churn flow regimes, as the experimental system was designed to avoid these flow conditions.

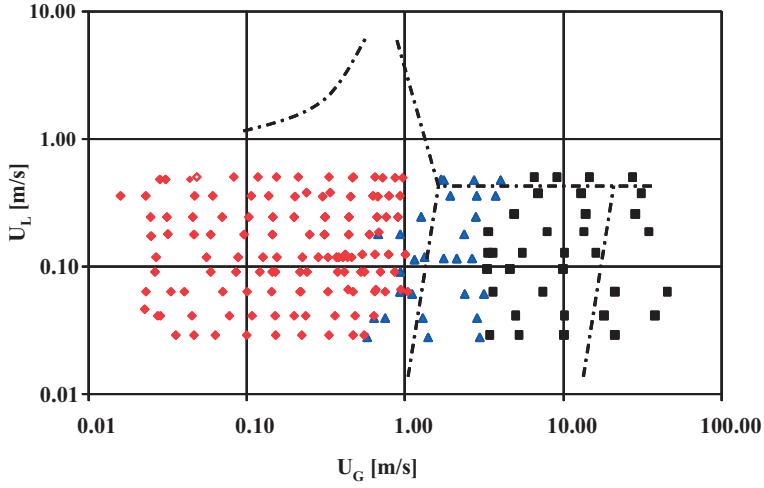

Figure 2. Flow regime map obtained for N_2-ethanol flow in a glass capillary, $d = 400\,\mu m$, adapted from [16]. Slug flow (◆); slug-annular flow (▲); annular flow (■); flow transition lines from [13] (– – –).

Following a detailed analysis of the literature data, Shao et al. [12] concluded that channel size, gas and liquid superficial velocities, liquid-phase surface tension, and channel wettability have the most significant effect on the position of the flow regime boundaries. The dependency of the flow regime transitions on the process conditions had already been remarked by other researchers. Akbar et al. [20] and Waelchli and von Rohr [15] proposed universal flow regime maps based on dimensionless numbers. Akbar et al. [20] suggested the use of gas and liquid Weber numbers, which take into account phase velocity, channel size, fluid density, and surface tension as coordinates of the flow regime map. On this basis, the comparison of literature data on air-water flows in circular and near-circular channels with dimensions of ~1 mm showed very good agreement as indicated in Fig. 3. However, this may not always be the case, as demonstrated in Fig. 4 by Shao et al. [12]. They reported relatively poor agreement between the flow map proposed by Akbar et al. [20] and other experimental data where

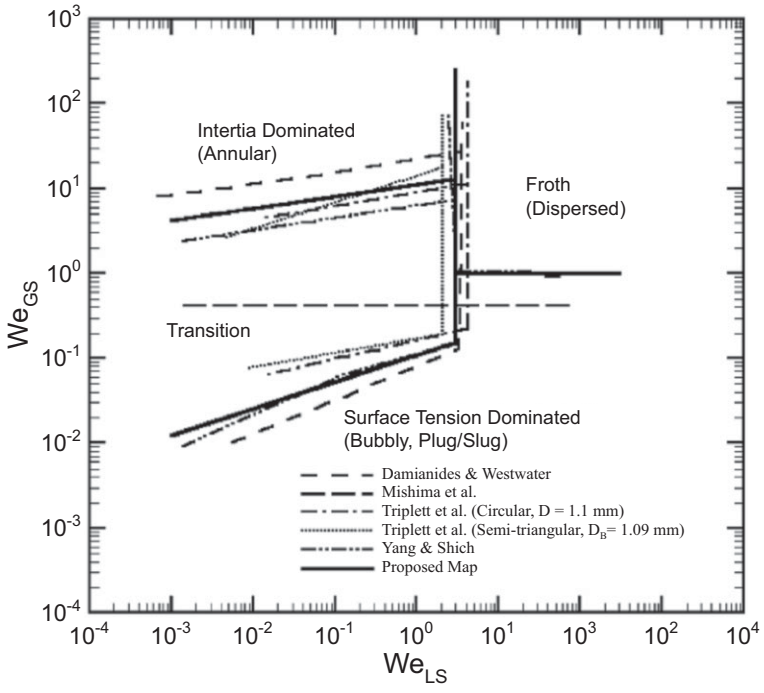

Figure 3. Universal flow map for gas-liquid flow in microchannels [20].

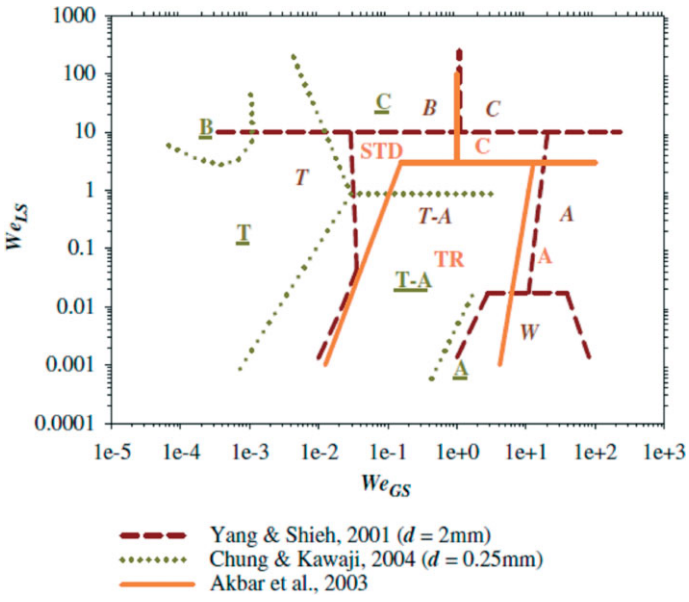

Figure 4. Comparison of the universal flow map for flow in tubes with diameters greater and smaller than 1 mm [12].

the channel sizes are relatively larger or smaller than 1 mm and fluids other than air and water are used. Another universal map is that proposed by Waelchli and von Rohr [15] which correlates the flow regimes using the Reynolds and Weber numbers as well as the surface roughness of the microchannel. Although the predicted transitions correspond well with the authors' experimental data, only three flow regimes (bubbly, Taylor ,and annular flow) are accounted for and, therefore, do not correspond well with a number of other experimental data.

It is apparent that no single universal map, which is independent of fluid and microchannel characteristics, has successfully been derived for the prediction of gas-liquid flow regimes. However, the number of studies on this topic is significant and the compiled data as well as the various flow regime predictions available do allow the correct order of magnitude of phase velocities to be selected for a required flow regime. If the boundaries between flow patterns are considered as transition zones that occupy a finite area on the flow regime map, then it should be possible to correctly predict a particular flow pattern, provided that the conditions do not fall too close to the boundaries of the flow transition lines.

2.2 Taylor Flow

Amongst the different gas-liquid flow regimes in microchannels, Taylor flow – or slug flow – is one of the most interesting flow regimes for chemical engineering applications. In addition to the fact that this flow regime is obtainable for a large range of gas and liquid flow rates, it is also characterized by a high gas-liquid interfacial area for mass transfer and relatively large bubble sizes which facilitates phase separation. Moreover, circulatory flow patterns exist in the liquid slug that allow good radial heat and mass transport as well as low axial diffusion, making this flow regime highly adapted to applications that involve heat and mass transfer between the gas and liquid and/or the liquid and channel wall [1, 22]. Over recent years, important work has been dedicated to Taylor flow in order to better understand the hydrodynamics, heat and mass transfer occurring in such flows, and how it enhances transport phenomena.

2.2.1 Bubble and Slug Lengths

The length of bubbles and slugs in Taylor flow has a direct impact on the performance of the gas-liquid application since the size of the liquid slug, which plays an important role in the rate of liquid recirculation, and the gas and liquid volume fractions directly affect heat and mass transfer. The dependency of bubble and slug lengths on operating parameters in both small tubes and microchannels have been studied experimentally and numerically by various researchers [16, 23–29], and a number of different empirical correlations – often based on phase holdup and dimensionless numbers (i.e., Re, Ca, We) – have been proposed. The agreement between these different correlations, however, is not always satisfactory. This is attributed to the fact that different inlet geometries with or without premixing have been employed since the bubble and slug lengths are strongly dependent on the size and the type of the inlet.

Therefore, the understanding of the bubble generation mechanism and the role of inlet geometry is highly important for correct prediction of bubble (and slug) lengths, and several studies have focused on this subject [30–34]. Garstecki et al. [30] proposed the *squeezing* mechanism for Taylor bubble formation in T-junctions when Ca <0.02 such that the interfacial forces dominate the shearing forces and when inertia is negligible (Re <1). Bubble generation is controlled by the pressure drop across the forming bubble and is composed of two stages: the filling stage where the bubble fills the main channel, and the squeezing stage where the liquid flow starts squeezing the bubble neck until pinch-off. Based on the characteristic times for the filling and squeezing stages, they proposed a simple model for bubble length:

$$\frac{L_G}{w} = \alpha_1 + \alpha_2 \frac{U_G}{U_L} \quad (1)$$

where $\alpha_1 \approx L_{G,fill}/w$ and $\alpha_2 \approx w_{in}/w$.

Van Steijn et al. [31] improved this model by taking into account the leakage flow that occurs around the forming bubble in rectangular channels and that increases the bubble size. For microchannels with square cross section, they found that the coefficients $\alpha_1 = \alpha_2 = 1.5$. The same authors later developed a complete predictive model for the size of bubbles and droplets generated in rectangular microchannels of arbitrary dimensions and demonstrated how the parameters α_1 and α_2 depend on the dimensions of the T-junction [32].

Pohorecki and Kula [35] later proposed a *switching* mechanism for the formation of Taylor bubbles in Y-junction microchannels and, consequently, a simple model for the prediction of bubble sizes.

$$\frac{L_G}{d} \sim 1 + \frac{U_G}{U_L} \quad (2)$$

This model is almost identical to the formulation given by Garstecki et al. [30] with the difference that the gas-to-liquid inlet width ratio is not explicitly taken into account in Eq. (2) since the gas and liquid inlets had the same dimensions. Furthermore, it is interesting to point out that this model was shown to correctly represent experimental bubble lengths obtained in microchannels with both square and circular cross sections and for varying fluid properties for conditions: $10 < Re < 350$ and $Ca << 1$ [16]. The model is also in very good agreement with the correlation provided by Qian and Lawal [28] through their numerical work that underlines the predominant effect of the flow rate ratio on the bubble length compared with the effects of surface tension and viscosity.

In sum, the above presented studies are in good agreement with one another and demonstrate that the size of Taylor bubbles is independent of the fluid properties and is a function of the microchannel geometry and the gas-to-liquid flow rate ratio only. This is of course true in the squeezing regime only when Ca <0.02 and inertia is negligible. For Ca >0.02, however, the shear stresses start to play a non-negligible role in the breakup process. Here, the bubbles are generated in the shearing regime and their size is controlled by the capillary number [33]. The transitional regime between the squeezing regime and the shearing regime is characterized by both, the pressure drop across the bubble (or drop) and the shear stresses [33, 36–38]. Consequently, these authors have demonstrated that the bubble size correlates with a combination of the gas-to-liquid flow rate ratio and the capillary number. The limit between the squeezing and shearing regimes is, however, not well defined: several authors have found the values of the critical capillary number to be around 0.002–0.006 (e.g., [36, 37, 39]), which is an order of magnitude lower than values defined by Garstecki et al. [30] and de Menech et al. [33]. This highlights that the effects of fluid properties most probably cannot be neglected for a large range of operating conditions when predicting the bubble size for process engineering applications. It is also interesting to point out that most studies on bubble (or drop) sizes do not consider the effects of inertia of the flow. Yet, even at very low capillary numbers ($\sim 10^{-4}$) with a small amount of inertia ($1 < Re < 10$), the bubble generation mechanism is modified and shows no negligible dependency on fluid properties [40].

2.2.2 Hydrodynamics in the Liquid Slug

A characteristic feature of gas-liquid Taylor flow is the recirculation motion created within the liquid slugs due to the difference in the bubble and liquid velocities. In the frame of reference of the bubble, this is described by stagnation points at the bubble nose and tail, which cause flow reversal and the creation of a recirculation motion along the length of the liquid slug as indicated in Fig. 5. This behavior – which was first postulated by Taylor [41] in 1961 and has since been confirmed by a number of experimental studies using particle image velocimetry (PIV) [15, 42–45] and computational investigations [46–49] – is the origin of the intensified mixing [43], heat [22, 50] and mass transfer [51–53] observed in such systems.

In a straight channel, the toroidal recirculation loop is symmetrical about the channel center line, and the radial position of the center of the loop center varies as a function of the capillary number. As Ca increases, the center of the recirculation

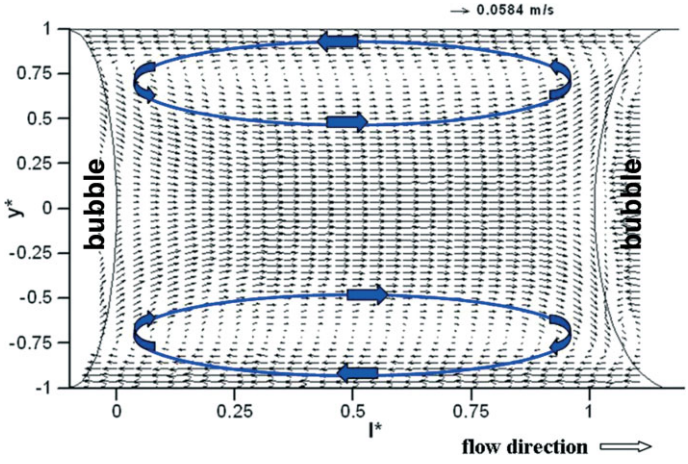

Figure 5. Recirculation flow patterns in a liquid slug of gas-liquid Taylor flow measured by micro-PIV [54].

loop moves towards the channel center line, thereby reducing the effective volume of recirculating liquid until the recirculation motion vanishes and total bypass flow occurs [42, 46, 55]. The rate of recirculation in the liquid slug has also shown to be highly dependent on the liquid slug length and the two-phase superficial velocity [42, 45]. These researchers have demonstrated that the recirculation rate increases with decreasing slug length and increasing two-phase superficial velocity. The results suggest that short, fast-moving liquid slugs are preferential for intensifying transport processes. However, the limits to this claim still need to be identified. An increase in two-phase velocity decreases the slug residence time, thus the time for transfer, and it also may have some impact on the liquid film thickness and effective recirculation volume. In heat transfer applications, if the liquid slug is too short, heat transfer may be hindered due to the dominating gas holdup [22].

When the gas-liquid Taylor flow passes through channel bends, the hydrodynamics in the liquid slug are significantly modified compared with the flow in a straight channel [43–45, 49]. Fig. 6 indicates that the recirculating flow is no longer symmetrical about the channel axis and the loops vary in size. Transverse flow (normal to the streamwise direction) is generated in the bend due to centrifugal forces [56]. The combination of this transverse flow with the recirculation loops creates a highly complex flow, which has shown to intensify mixing in the slug significantly [43] and provides narrow residence time distributions [57]. Fries et al. [44] and Fries and von Rohr [49] have also reported that the asymmetry of the recirculation loops and the strength of recirculation depend on microchannel geometry (dimensions, radius of curvature) as well as on the superficial velocities of the gas and liquid phases. Although these studies have shown the development of complex flow behavior in microchannels bends, a complete description and analysis of the flow in three dimensions is still required.

2.2.3 Liquid Film

Besides the lengths of bubbles and slugs in Taylor flow, the description of the liquid film that surrounds the bubble body is important. The existence of this thin liquid film plays an important role in the hydrodynamics and transport phenomena. There are a number of expressions given in the literature for the calculation of δ, the thickness of the *lubricating* film. The most commonly used correlations are those proposed by Bretherton [58], Schwartz et al. [59], and Aussillous and Quéré [60] for the flow in cylindrical capillary tubes:

$$\frac{\delta}{d} = 0.67\mathrm{Ca}^{\frac{2}{3}} \quad \text{for Ca} \ll 10^{0} \text{ and negligible inertial effects} \quad (3)$$

$$\frac{\delta}{d} = 0.25\mathrm{Ca}^{\frac{1}{2}} \quad \text{for Ca} < 10^{-3} \quad (4)$$

$$\frac{\delta}{d} = \frac{0.67\mathrm{Ca}^{\frac{2}{3}}}{1 + 3.33\mathrm{Ca}^{\frac{2}{3}}} \quad \text{for Ca} < 10^{0} \text{ and negligible inertial effects} \quad (5)$$

In cylindrical geometries where the effects of gravity and inertia can be neglected, the liquid film around the bubble has a constant thickness, which increases with the capillary number. Pohorecki and Kula [35] compared the values of the liquid film thickness returned by Eqs. (3)–(5), as indicated in Tab. 1. It can be seen that for small values of Ca (~10^{-3}), all three expressions are in reasonable agreement. However, for higher Ca (10^{-2}–10^{-1}), only expressions (4) and (5) are in good agree-

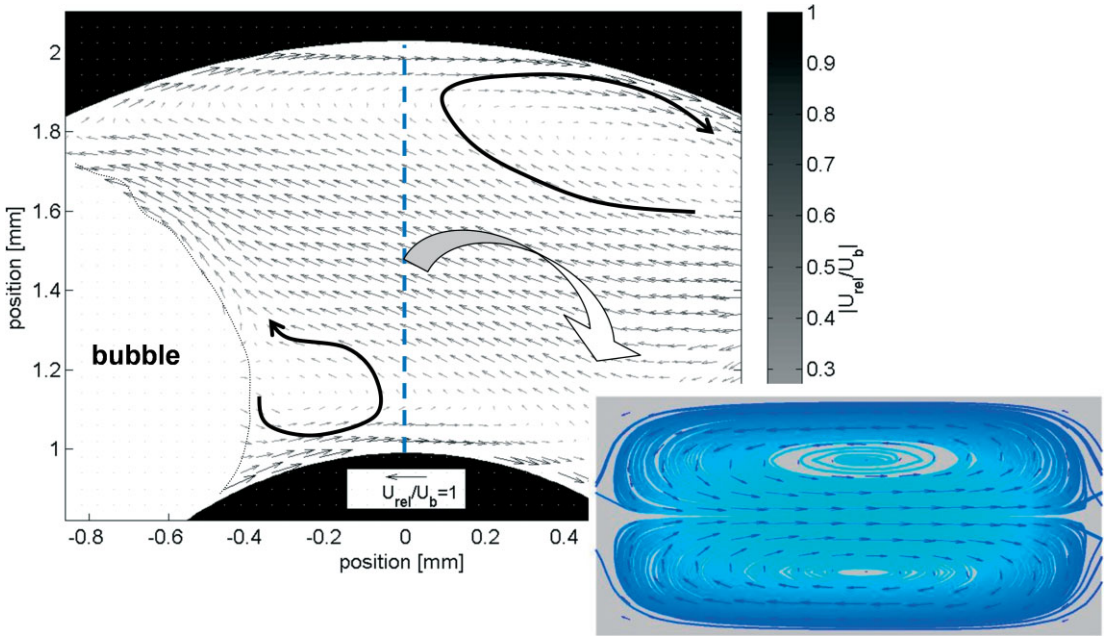

Figure 6. Recirculation flow patterns (reference frame of the bubble) between two Taylor bubbles in a microchannel bend. Inset: transverse flow patterns in single-phase flow induced in the channel bend.

Table 1. Comparison of the values of relative lubricating film thickness, δ/d, calculated using different literature expressions.

Ca / Expression	10^{-3}	10^{-2}	10^{-1}	10^{0}
$\frac{\delta}{d} = 0.67\mathrm{Ca}^{\frac{2}{3}}$	0.0067	0.031	0.145	0.67
$\frac{\delta}{d} = 0.25\mathrm{Ca}^{\frac{1}{2}}$	0.008	0.025	0.08	0.25
$\frac{\delta}{d} = \frac{0.67\mathrm{Ca}^{\frac{2}{3}}}{1+3.33\mathrm{Ca}^{\frac{2}{3}}}$	0.0064	0.026	0.083	0.152

ment, since they have been corrected for higher capillary numbers.

In the case of non-negligible inertia, several researchers have reported that for a constant capillary number, the liquid film thickness first decreases and then increases with increasing Reynolds number [61–63]. Han and Shikazono [63] have demonstrated that for $\mathrm{Ca} \geq 10^{-2}$ the inertial force influences the liquid film thickness around the bubbles. For low and constant values of Ca, the dimensionless liquid film thickness does not vary with increasing Re, as predicted by Eqs. (3)–(5). However, for constant Ca at values $\geq 10^{-2}$, the liquid film globally increases with increasing Re. Consequently, the authors proposed two correlations based on the Ca, Re, and We:

$$\frac{\delta}{d} = \frac{0.670\ \mathrm{Ca}^{\frac{2}{3}}}{1 + 1.13\ \mathrm{Ca}^{\frac{2}{3}} + 0.504\ \mathrm{Ca}^{0.672}\mathrm{Re}^{0.589} - 0.352\ \mathrm{We}^{0.629}} \quad \mathrm{Re} < 2000$$

$$\frac{\delta}{d} = \frac{106.0\ \left(\frac{\mathrm{Ca}}{\mathrm{Re}}\right)^{\frac{2}{3}}}{1 + 497.0\ \left(\frac{\mathrm{Ca}}{\mathrm{Re}}\right)^{\frac{2}{3}} + 7330\ \left(\frac{\mathrm{Ca}}{\mathrm{Re}}\right)^{0.672} - 5000\ \left(\frac{\mathrm{Ca}}{\mathrm{Re}}\right)^{0.629}} \quad \mathrm{Re} > 2000 \tag{6}$$

The interest in monolith reactors in the early 1990s and in microreactors more recently has led a number of researchers to investigate the liquid film around Taylor bubbles in square [19, 23, 47, 55, 64–66] and rectangular channels [67, 68]. Due to the presence of the channel corners, the liquid film thickness around the bubble varies. Kreutzer et al. [47] presented a correlation for the film thickness in the diagonal direction of a square channel via the dimensionless bubble diameter such that:

$$\frac{\delta_\mathrm{d}}{d_\mathrm{H}} = \frac{\sqrt{2}}{2} - 0.35 - 0.25\exp(-2.25\mathrm{Ca}^{0.445}) \tag{7}$$

From this equation it can be concluded that with $\mathrm{Ca} \to 0$, $\delta_\mathrm{d}/d_\mathrm{H}$ tends towards a value of 0.107, i.e., the bubble never occupies the entire cross section of the channel and there is always liquid in the corners. Furthermore, the correlation indicates that the film thickness is dependent only on the capillary number, thereby assuming negligible inertial effects.

Han and Shikazono [66] extended their experimental work in circular capillaries to square cross-sectional microchannels and developed a correlation for the effects of inertia on the liquid film thickness in the channel corner δ_d and the center edge δ_c:

$$\frac{\delta_\mathrm{d}}{d_\mathrm{H}} = 0.122 + \frac{1.22\mathrm{Ca}^{2/3}}{1 + 7.28\mathrm{Ca}^{2/3} - 0.255\mathrm{We}^{0.215}} \quad \mathrm{Re} < 2000$$

$$\frac{\delta_\mathrm{d}}{d_\mathrm{H}} = 0.122 + \frac{1934\left(\frac{\mathrm{Ca}}{\mathrm{Re}}\right)^{2/3}}{1 + 1.156\left(\frac{\mathrm{Ca}}{\mathrm{Re}}\right)^{2/3} - 6.70\left(\frac{\mathrm{Ca}}{\mathrm{Re}}\right)^{0.215}} \quad \mathrm{Re} \geq 2000 \tag{8}$$

$$\frac{\delta_\mathrm{c}}{d_\mathrm{H}} \approx 0 \quad \text{for } \frac{\delta_\mathrm{d}}{d_\mathrm{H}} < \frac{\sqrt{2}-1}{2}$$
$$\frac{\delta_\mathrm{c}}{d_\mathrm{H}} = \frac{\delta_\mathrm{d}}{d_\mathrm{H}} \quad \text{for } \frac{\delta_\mathrm{d}}{d_\mathrm{H}} \geq \frac{\sqrt{2}-1}{2} \tag{9}$$

According to Eq. (8), as Ca approaches zero and inertia becomes negligible, the dimensionless liquid film thickness in the channel corner tends to a value of 0.122 which is very similar to the limiting value predicted by Eq. (7).

Few studies have focused on the liquid film thickness around bubbles in rectangular cross-sectional microchannels. It is expected that the film thickness at the lateral walls differs from that above and below the bubble, depending on the aspect ratio of the microchannel [69, 70], and these differ of course from the diagonal film thickness. Furthermore, when inertial effects are non-negligible, the film thickness also varies axially from the bubble nose to tail [68]. Yun et al [68] presented two correlations from their experimental data for the minimum and maximum values of the lateral liquid film thickness along the length of the bubble:

$$\frac{\delta_\mathrm{min}}{d_\mathrm{H}} = 0.02\,\mathrm{We}^{0.62}$$
$$\frac{\delta_\mathrm{max}}{d_\mathrm{H}} = 0.39\,\mathrm{We}^{0.09} \tag{10}$$

2.2.4 Pressure Drop

The total pressure drop of gas-liquid flows in microchannels includes four different values [71]:

$$\Delta P_\mathrm{T} = \Delta P_\mathrm{A} + \Delta P_\mathrm{B} + \Delta P_\mathrm{G} + \Delta P_\mathrm{F} \tag{11}$$

where
ΔP_A is the pressure drop due to acceleration [17]:

$$\Delta P_\mathrm{A} = G^2\left[\left(\frac{x^2}{\varepsilon_\mathrm{G}\rho_\mathrm{G}} + \frac{(1-x)^2}{(1-\varepsilon_\mathrm{G})\rho_\mathrm{L}}\right)_\mathrm{outlet} - \left(\frac{x^2}{\varepsilon_\mathrm{G}\rho_\mathrm{G}} + \frac{(1-x)^2}{(1-\varepsilon_\mathrm{G})\rho_\mathrm{L}}\right)_\mathrm{inlet}\right] \tag{12}$$

ΔP_B is the pressure drop over a moving bubble due to a change of shape of the bubble front and bubble tail [58]:

$$\Delta P_\mathrm{B} = 3.58\frac{\sigma}{d/2}\sqrt[3]{9\mathrm{Ca}^2} \tag{13}$$

ΔP_G is the pressure drop due to gravity [71]:

$$\frac{\Delta P_G}{L} = (\varepsilon_G \rho_G + (1-\varepsilon_G)\rho_L) g \sin(\alpha) \tag{14}$$

ΔP_F is the frictional pressure drop [17]:

$$\frac{\Delta P_F}{L} = f \rho_L u_{TP}^2 \frac{2}{d} \varepsilon_L \tag{15}$$

The pressure drop contributions defined by Eqs. (12)–(14) can be simply calculated from the experimental conditions. Under simplifying assumptions – quasi-homogeneous mixture or combination of the gas and liquid pressure drops using fitted experimental multipliers, respectively – the frictional pressure drop may be determined using the homogeneous or Lockhart-Martinelli models. Lockhart and Martinelli [72] proposed that the pressure drop in two-phase flow can be related to the equivalent pressure drop in single-phase flow using a two-phase parameter Φ:

$$\left(\frac{\Delta P_F}{L}\right)_{TP} = \phi_L^2 \left(\frac{\Delta P_F}{L}\right)_L = \phi_G^2 \left(\frac{\Delta P_F}{L}\right)_G \tag{16}$$

where Φ_L is correlated as [73]:

$$\phi_L^2 = 1 + \frac{C}{X} + \frac{1}{X^2} \tag{17}$$

and X is the ratio:

$$X^2 = \frac{\left(\frac{\Delta P_F}{L}\right)_L}{\left(\frac{\Delta P_F}{L}\right)_G} \tag{18}$$

The main difficulty encountered with the Lockhart-Martinelli model is the determination of the C-factor. Tab. 2 summarizes different C-factor correlations used for laminar gas-liquid flows.

Tab. 3 presents a comparison of the C-factor values obtained for a water-nitrogen system in a microchannel ($d = 0.4 \cdot 10^{-3}$ m) using the above correlations. It can be seen that the correlations from [73, 74, 76] are in a reasonable agreement, whereas the correlation of Lee and Lee [75] approaches the other correlations only for the highest values of the Re and Ca numbers. According to the present authors' experience, the correlation of Sairson and Wongwises [76] may be recommended.

Table 2. C-factor correlations for microchannels.

Author	C-factor correlation
Chisholm [73]	$C = 5$
Mishima and Hibiki [74]	$C = 21[1-e^{(-319d)}]$
Lee and Lee [75]	$C = 6.833 \cdot 10^{-8} \lambda^{-1.317} \mathrm{Re}^{0.557} \mathrm{Ca}^{0.719}$ $\lambda = \frac{\mu_L^2}{\rho_L \sigma d}$
Sairson and Wongwises [76]	$C = 7.599 \cdot 10^{-3} \lambda^{-0.631} \mathrm{Re}^{0.008} \mathrm{Ca}^{0.005}$

It should be pointed out that the simplifying assumptions associated with both traditional models (homogeneous and Lockhart-Martinelli) are rather unrealistic in the case of Taylor flow. However, these models allow a correct order of magnitude estimation of the pressure drop with data that is simple to retrieve. A more rational approach (ignoring the pressure drop in the bubble regions, applying the Hagen-Poiseuille law for the slug regions, and adding the Laplace pressure term) has been given by Kreutzer and co-workers [47, 102]. However, this approach requires the knowledge of the slug length which renders it less practical from the engineering and industrial point of view. For this reason we limited our analysis to the two traditional models.

2.2.5 Mass Transfer

An important advantage of microreactors for gas-liquid reactions is the significant intensification of the mass transfer processes. For illustration, a comparison of the characteristic values governing gas-liquid mass transfer in a variety of conventional equipment and microreactors is given in Tab. 4 from Yue et al. [51]. The values in this table indicate that the volumetric mass transfer coefficient, $k_L a$, is 10^1–10^2 times greater in microreactors compared with that in conventional process equipment. However, it is interesting to point out that this intensification of mass transfer is principally due to a huge increase in the specific interfacial area in microstructured devices. The mass transfer coefficient itself is of the same order of magnitude as that obtained in static mixers and tubular reactors.

As mentioned earlier, the most interesting regime of the gas-liquid flow in a microreactor is Taylor or slug flow. In this regime, a number of contributions to the mass transfer processes may be distinguished as demonstrated in Fig. 7 and listed as: (1) bubble to wall through film; (1a) bubble to film;

Table 3. Comparison of the values of the C-factor calculated using the various literature expressions.

Re	10			100			1000		
Ca	10^{-3}	10^{-2}	10^{0}	10^{-3}	10^{-2}	10^{0}	10^{-3}	10^{-2}	10^{0}
Chisholm [73]	5	5	5	5	5	5	5	5	5
Mishima and Hibiki [74]	2.5	2.5	2.5	2.5	2.5	2.5	2.5	2.5	2.5
Lee and Lee [75]	$6.4 \cdot 10^{-4}$	$3.4 \cdot 10^{-3}$	0.091	$2.3 \cdot 10^{-3}$	0.012	0.33	$8.2 \cdot 10^{-3}$	0.043	1.19
Sairson and Wongwises [76]	3.4	3.4	3.5	3.3	3.3	3.4	3.2	3.3	3.4

Table 4. Comparison of mass transfer parameters in different gas-liquid contactors from Yue et al. [51].

Type of contactor	$k_L \cdot 10^5$ [m s^{-1}]	a [m^{2}m^{-3}]	$k_L a \cdot 10^2$ [s^{-1}]
Bubble columns	10–40	50–600	0.5–24
Couette-Taylor flow reactor	9–20	200–1200	3–21
Impinging jet absorbers	29–66	90–2050	2.5–122
Packed columns, concurrent	4–60	10–1700	0.04–102
Packed columns, countercurrent	4–20	10–350	0.04–7
Spray column	12–19	75–170	1.5–2.2
Static mixers	100–450	100–1000	10–250
Stirred tank	0.3–80	100–2000	3–40
Tube reactors, horizontal and coiled	10–100	50–700	0.5–70
Tube reactors, vertical	20–50	100–2000	2–100
Gas-liquid microchannel	40–160	3400–9000	30–2100

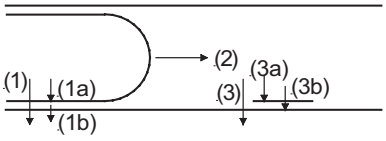

Figure 7. Mass transfer contributions in the Taylor flow.

(1b) film to wall; (2) bubble to slug; (3) slug to wall; (3a) slug to film; (3b) film to wall.

If the channel wall takes part in the mass transfer process (i.e., due to an *active wall* that is coated with a catalyst, for example), then all the above-mentioned contributions may occur simultaneously [101]. On the other hand, if the microchannel wall is a *passive wall*, then only processes (1a) and (2) will occur [103–105].

Van Baten and Krishna [77] proposed that the gas-to-liquid mass transfer process may be described as:

$$k_L a = k_{LC} a_C + k_{LF} a_F \tag{19}$$

According to this approach, the overall gas-liquid interfacial area is composed of two parts: the area of bubble ends, or caps (a_C), and the area of the lubricating film between the bubble and the channel wall (a_F) [58–60, 78]. This distinction of these two parts is very important since the contribution of the lateral interfacial area, i.e., at the liquid film, to the total interfacial area may exceed 90 %. Since the lubricating layer is usually very thin (~10^{-6} m), it is easily saturated with the absorbed component or exhausted of the liquid-phase reactant, and thus may cease to contribute actively to the mass transfer process. A criterion that enables to identify whether the film contributes to the mass transfer or not was developed by Pohorecki [78].

Older correlations for the mass transfer coefficients did not differentiate between the above-described regions. In an early study, Bercic and Pintar [79] proposed an empirical correlation for the $k_L a$ based on experimental studies of the absorption of methane in water using circular capillaries of 1.5, 2.5, and 3.1 mm diameter. They found that $k_L a$ is dependent on both the gas and liquid superficial velocities as well as the length of the unit cell ($L_G + L_L$).

$$k_L a = 0.111 \frac{(U_G + U_L)^{1.19}}{((1-\varepsilon_G)(L_G + L_L))^{0.57}} \tag{20}$$

In another study, Vandu et al. [80] investigated the absorption of oxygen (from an O_2/N_2 mixture) in water using capillaries of square and circular cross sections (diameter 1, 2, or 3 mm). They put forward an empirical correlation for $k_L a$ indicating that it is dependent on the gas and liquid superficial velocities, the unit cell length, and also the liquid phase diffusivity.

$$k_L a = 4.5 \sqrt{\frac{D\, U_G}{L_G + L_L}}\, \frac{1}{d} \tag{21}$$

More recently, Yue et al. [51] measured the rate of pure CO_2 absorption into a buffer solution of $K_2CO_3/KHCO_3$ in a Y-type rectangular microchannel (1 mm deep, 0.5 mm wide). They proposed a correlation for $k_L a$ using the Sherwood (Sh), Schmidt (Sc), and Reynolds numbers for the liquid phase and the Reynolds number for the gas phase.

$$\mathrm{Sh_L}\; a\; d = 0.084\; \mathrm{Re_G^{0.213}} \mathrm{Re_L^{0.937}} \mathrm{Sc_L^{0.5}} \tag{22}$$

Sobieszuk et al. [52] measured the CO_2 rate of absorption from the CO_2/N_2 mixture into a buffer solution of $K_2CO_3/KHCO_3$ in a Y-type capillary (0.4 mm diameter). They obtained lower values of $k_L a$ than those calculated from the Bercic and Pintar [79] and Vandu et al. [80] correlations. However, very good agreement was observed with the data of Yue et al. [34] for lower values of the apparent liquid velocity. Nevertheless, Yue et al. [51] observed a much stronger influence of liquid velocity. Yue et al. [81] further proposed another correlation for $k_L a$:

$$k_L a = \frac{2}{d} \left(\frac{D\, U_G}{L_G + L_L} \right)^{0.5} \left(\frac{L_G}{L_G + L_L} \right)^{0.3} \tag{23}$$

This correlation, based on experiments performed for a square cross-sectional microreactor with a hydraulic diameter of 0.4 mm, gave somewhat higher $k_L a$ values, but still in the same range.

Sobieszuk et al. [53] measured the interfacial area for gas-liquid Taylor flow in a microchannel of 0.4 mm diameter using Danckwerts' chemical method (a_D). The physicochemical system investigated was CO_2 absorption from a CO_2/N_2 mixture into a $K_2CO_3/KHCO_3$ aqueous buffer solution containing a hypochlorite catalyst. They also measured the interfacial area by a photographic method. This allowed the film (a_F) and caps' (a_C) interfacial area values to be determined independently. The total interfacial area (a_T) is the sum of a_F and a_C. Fig. 8 demonstrates a reasonable agreement of the values determined geometrically using high-speed photography and those obtained using Danckwerts' chemical method.

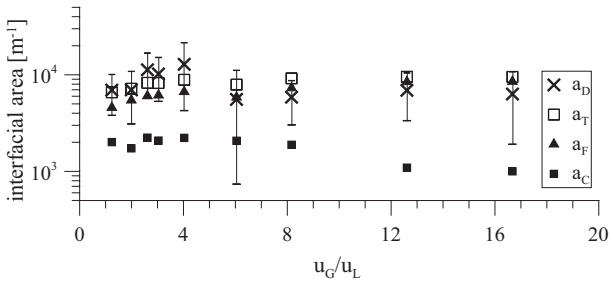

Figure 8. Comparison of interfacial area values obtained by Danckwerts' and photographic methods; error bars mean the 95 % confidence limits [53].

Sobieszuk et al. [53] also were able to determine the values of k_{LF} and k_{LC} separately. As the experimental values k_{LC} and k_{LF} were found to be very close, the authors chose to correlate them in a traditional way, using the Sh, Re, and Sc:

$$\mathrm{Sh} = 0.1\,\mathrm{Re}^{1.12}\mathrm{Sc}^{0.05} \tag{24}$$

Sobieszuk et al. [53] also compared their own experimental data obtained by means of chemical and physical absorption methods with the literature correlations (Eqs. (20)–(23)), as presented in Fig. 9. The correlations of Bercic and Pintar [79] and of Vandu [80] give definitely higher values of the volumetric mass transfer coefficient, whereas those of Yue et al. [51, 81] ndash; although differing from each other – are closer to the results obtained by Sobieszuk et al. [52, 53]. Taking into account that the data from Sobieszuk et al. [52, 53] have been obtained using both physical and chemical methods and are close to the newest data of Yue et al. [81], these data are to be recommended.

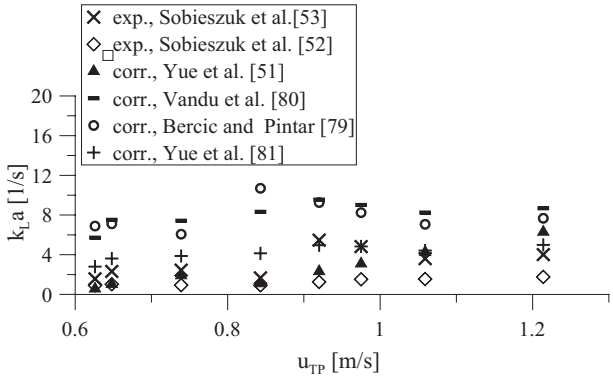

Figure 9. Comparison of different k_La values in microchannels [53].

Van Baten and Krishna [82] simulated liquid-to-wall mass transfer for Taylor flow in circular capillaries. Based on 46 simulations, they proposed a correlation for liquid-to-wall mass transfer coefficients:

$$\mathrm{Sh_w} = \frac{\beta}{\mathrm{Gz}_{\mathrm{tube}}^{a}}\ ,\quad a = 0.61\ \mathrm{Gz}_{\mathrm{slug}}^{0.025}$$
$$\beta = \frac{0.5}{\left(\mathrm{Gz}_{\mathrm{slug}}/\varepsilon_G\right)^{0.15}}\ ,\quad \mathrm{Gz}_{\mathrm{slug}} = \frac{L_L\ D}{d^2\ U_b} \tag{25}$$

valid in the range $\mathrm{Gz}_{\mathrm{tube}} < 0.01$ which is most important from a practical point of view. The above correlation is in reasonably good agreement with earlier experimental measurements by Bercic and Pintar [79] and Horwath et al. [93]. However, further research on liquid-to-wall mass transfer would be desirable.

3 Open-Channel Microreactors

Open microchannels typically have the form of grooves etched or cut in a flat plate and are open from one side to ensure contact with the other phase. A typical example of an open microchannel apparatus is the falling-film microreactor (FFMR; Fig. 10). In the FFMR, a thin film of liquid trickles over the grooves due to gravitational forces and is open to the gas phase.

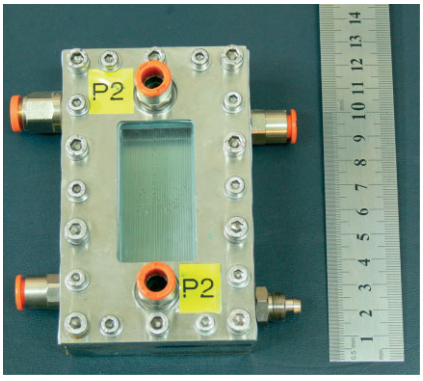

Figure 10. Falling-film microreactor, produced by the Institut für Mikrotechnik Mainz GmbH.

3.1 Hydrodynamics

The hydrodynamics of the gas phase flow in FFMRs has received relatively little attention. Commenge et al. [83] investigated the gas-phase residence time distribution (RTD) in an FFMR and observed that the formation of recirculation loops at the gas inlet and a jet effect considerably increased the mixing within the gas phase. They used a tank-in-series model for the gas mixing and found that the number of CSTRs (continuous stirred-tank reactors) is a simple function of the gas Reynolds number.

As opposed to the gas flow, the hydrodynamics of liquid flow in FFMR have been more intensively investigated. Yeong et al. [84] measured the film thicknesses using reflection confocal microscopy and observed different cross-sectional profiles of the liquid film surface at various flow rates and in different microchannels. The influence of the contact angle on the liquid profile in microchannels was examined as illustrated in Fig. 11 [85, 86].

According to Zhang et al. [86], the increase of interfacial due to this effect may exceed 50 %. However, for contact angle values higher than 30° it does not exceed 20 %. Monnier at al. [87] investigated the film stability in FFMRs. They observed that when the liquid flow rate is lower than the minimal liquid

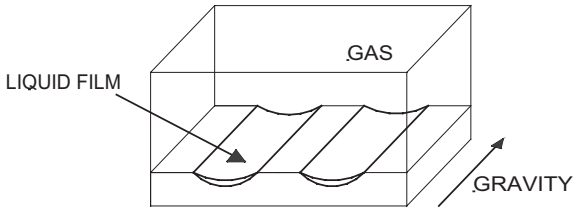

Figure 11. Schematic view of the microstructured plate [85].

flow rate, the film breaks into rivulets. Zhang et al. [86] proposed a means to approximate the liquid film thickness following the Nusselt theory:

$$\delta = \sqrt[3]{\frac{3\ Q_L \nu_L}{n\ w\ g}} \tag{26}$$

However, this theory was developed for a flat plate, and underestimates the film thickness in a groove or channel as explained above.

3.2 Mass Transfer

Only recently studies have been devoted to gas-liquid mass transfer in FFMRs. Commenge et al. [8] and Sobieszuk and Pohorecki [89] measured the gas-side mass transfer coefficients k_G via the absorption of SO_2 and pure CO_2 in NaOH solutions, respectively. The measured k_G were in the range of 10^{-3}–10^{-2} m s^{-1}, strongly depending on the gas velocity as predicted by the correlation proposed by Obein [94]:

$$Sh_G = 0.37\ Re_G^{0.84}\ Sc_G^{1/3} \tag{27}$$

For lower values of gas velocity, Sobieszuk and Pohorecki [89] observed also a slight increase of the mass transfer coefficient with increasing liquid flow rate and explained this by the fact that the gas phase may be accelerated by the liquid flow.

The liquid-side mass transfer coefficient in FFMRs has been investigated using both experimental and computational techniques. Zanfir et al. [90] firstly modeled the process of CO_2 absorption into sodium hydroxide solutions using a 2D model with no adjustable parameters, then compared the results with experimental data and found a good agreement. Chasanis et al. [91] and Al-Rawashdeh et al. [85] simulated the same system using a rigorous 2D model and a pseudo-3D model, respectively. Both approaches provided results which were in reasonably good agreement with the experimental data. The k_L values in an FFMR were measurement by Zhang et al. [86] and Sobieszuk et al. [92]. Both groups used a CO_2-NaOH system. The values obtained by both groups are in very good agreement and ranged from $7 \cdot 10^{-7}$ to $13 \cdot 10^{-5}$ m s^{-1}. This is somewhat higher than predicted by the Higbie formula:

$$k_L = 2\sqrt{\frac{D}{\pi\ \tau}} \tag{28}$$

Since the contact time between the gas and the liquid in FFMRs is relatively long, and, therefore, the liquid-side mass transfer coefficients are relatively low, an interesting question arises, whether the interfacial tension-driven cells may develop in the limited space of a microchannel. This phenomenon, which is called the Marangoni effect, might significantly increase the mass transfer rate. One way of approaching this problem is to measure the mass transfer rate in a microreactor using a system known to exhibit the Marangoni effect in the macroscale and to compare this rate with the value determined for the analogous process without this effect. Sobieszuk et al. [92] investigated the CO_2 absorption in aqueous solutions of monoethanolamine in an FFMR as a typical example of a process in which the Marangoni effect is observed in larger apparatus, e.g., wetted columns and packed columns. They found a significant enhancement (up to four times) of the absorption rate in the FFMR and concluded that convection cells can develop even in the limited space of a microchannel. Similar effects were observed in packed columns by Warmuzinski et al. [95].

4 Conclusions

A large number of studies have been dedicated to both gas-liquid hydrodynamics and mass transfer in microreactors and microstructured equipment. Most of these studies have focused on flows in closed microchannels (or small tubes), whilst open-channel devices, such as falling-film microreactors, have obtained less attention. Obviously, fundamental knowledge, especially in the area of closed-channel gas-liquid flows, already exists and many aspects are generally well understood. Nevertheless, some gaps in the knowledge are still remaining:

- Despite the large number of studies concerning characterization and prediction of gas-liquid flow regimes in closed microchannels, no completely universal flow map exists. Nevertheless, a large amount of data exists in this area thereby making it possible to select the correct order of magnitude of phase velocities for a required flow regime.
- Amongst the different flow regimes, Taylor flow is probably the most suitable for industrial applications due to the fact that it can be obtained for a wide range of flow conditions, it has a relatively high interfacial area, and it offers interesting flow patterns which promote heat and mass transfer processes.
- Simple mechanisms for the generation of Taylor flow have been proposed and allow a reliable prediction of bubble and slug lengths which depend uniquely on the gas and liquid flow rates and channel dimensions if the capillary number is low and inertial effects are negligible. However, when inertia cannot be neglected, the effects of fluid properties most probably cannot be neglected for a large range of operating conditions when predicting the bubble size for process engineering applications.
- The recirculation motion generated in the liquid slugs of Taylor flow in straight channels has been largely characterized by both experimental and numerical techniques. In meandering channels, this flow proved to become much more complex, however, the 3D aspects of this flow still require complete description and analysis. This may be possible with the development of 3D simulations or experimentally using advanced techniques such as stereo- or confocal micro-PIV.

– The liquid film thickness surrounding the body of the Taylor bubble in both circular and square cross-sectional channels (or tubes) has been extensively well documented and a number of correlations exist. The variations in film thickness in rectangular cross-sectional channels are not well characterized.
– The pressure drop in Taylor flow may be correctly estimated by the Lockhart and Martinelli model for engineering purposes despite the associated assumptions, and a number of correlations for the *C*-factor are available. For the *C*-factor, the correlation by Sairson and Wongwises [76] is recommended.
– The description of gas-to-liquid mass transfer in Taylor flow must take into account the contribution of two different regions: the bubble caps and the lubricating liquid film. The measurements of the interfacial area performed using both physical and chemical methods indicate that for a sufficiently high Reynolds number both regions are active in the mass transfer process.
– The liquid-side volumetric mass transfer coefficient obtained in microreactors is one to two orders of magnitude greater than in conventional equipment. This increase is predominantly due to an increase in the specific interfacial area available for the mass transport process.
– Characteristic information on the operation of open microchannel devices, and in particular FFMRs, is relatively scarce compared with closed-channel devices. The Nusselt formula can be used as the first approximation of the liquid film thickness in FFMRs, however, it underestimates the value in grooved plates by about 10–30 %.
– The values of the liquid-side and gas-side mass transfer coefficients in FFMRs are in the ranges of k_L from $7{\cdot}10^{-7}$ to $13{\cdot}10^{-5}$ m s^{-1} and k_G from 10^{-3} to 10^{-2} m s^{-1}, respectively. The k_L values may by significantly increased by the Marangoni (interfacial) effects.

Acknowledgment

The authors gratefully acknowledge financial support from the following programs: Integrated Project IMPULSE (FP6, grant no. NMP2-CT-2005-011816, 2005-2009), CNRS-France and ASCR-Czech Republic (grant no. 22540), ANR France (project MIGALI, grant no. ANR-09-BLAN-0381-01), and National Centre for Science, Poland (grant no. NN209 026 140). The authors would also like to thank various colleagues: C. Xuereb, N. Völkel, D. Legendre, T. Abadie, V. Jiricny, J. Kristal, P. Zaloha, P. Cyganski, J. Grzelka, M. Kraut, and F. Olschewski.

The authors have declared no conflict of interest.

Symbols used

a	[m^{2}m^{-3}]	interfacial area per unit channel volume
C	[–]	coefficient in the Lockhart-Martinelli model
Ca	[–]	capillary number, two-phase, $U_{TP}\mu L/\sigma$
d	[m]	diameter
D	[m^{2}s^{-1}]	diffusivity
f	[–]	friction factor
g	[m s^{-2}]	gravitational acceleration
Gz_{slug}	[–]	Graetz number for liquid slug, $L_L D/(d^2 U_b)$
Gz_{tube}	[–]	Graetz number for tube, $L(1–\varepsilon_G)D/(d^2 U_b)$
k_G	[m s^{-1}]	gas-side mass transfer coefficient
k_L	[m s^{-1}]	liquid-side mass transfer coefficient
k_S	[m]	surface roughness
k_W	[m s^{-1}]	liquid-to-wall mass transfer coefficient
L	[m]	channel length
L_G	[m]	bubble length
L_L	[m]	liquid slug length
n	[–]	number of microchannels
ΔP_A	[Pa]	pressure drop due to acceleration
ΔP_B	[Pa]	pressure drop due to change of shape of the bubble
ΔP_F	[Pa]	frictional pressure drop
ΔP_G	[Pa]	pressure drop due to the gravity
ΔP_T	[Pa]	total pressure drop
Q	[m^{3}s^{-1}]	flow rate
Re	[–]	Reynolds number, $U_{TP}d\rho_L/\mu_L$
Re_G	[–]	Reynolds number, gas phase, $U_G d\rho_G/\mu_G$
Re_L	[–]	Reynolds number, liquid phase, $U_L d\rho_L/\mu_L$
Sc_G	[–]	Schmidt number, gas phase, $\mu_G/(\rho_G D)$
Sc_L	[–]	Schmidt number, liquid phase, $\mu_L/(\rho_L D)$
Sh_G	[–]	Sherwood number, gas phase, $k_G d/D$
Sh_L	[–]	Sherwood number, liquid phase, $k_L d/D$
Sh_W	[–]	Sherwood number, liquid-to-wall, $k_W d/D$
U	[m s^{-1}]	superficial velocity
U_b	[m s^{-1}]	bubble velocity
w, w_{in}	[m]	width of microchannel, microchannel inlet
We	[–]	Weber number, two-phase, $U_{TP}{}^2 d\rho_L/\sigma$
We_G	[–]	Weber number, gas phase, $U_G{}^2 d\rho_L/\sigma$
We_L	[–]	Weber number, liquid phase, $U_L{}^2 d\rho_L/\sigma$
x	[–]	gas mass fraction
X	[–]	Lockhart-Martinelli parameter

Greek letters

α	[–]	parameter in Eq. (25), $\alpha = 0.61(Gz_{slug})^{0.025}$
α_1, α_2	[–]	parameters in Eq. (8)

β	[–]	parameter in Eq. (25), $\beta = 0.5(Gz_{slug}/\varepsilon_G)^{-0.15}$
δ	[m]	liquid film thickness
ε	[–]	holdup
λ	[–]	parameter, $\lambda = \mu_L^2/(\rho_L s d)$
ρ	[kg m^{-3}]	density
μ	[Pa s]	dynamic viscosity
σ	[N m^{-1}]	surface tension
τ	[s]	Higbie contact time
ν	[m^{2}s^{-1}]	kinematic viscosity
ϕ	[–]	two-phase multiplier in the Lockhart-Martinelli model

Subscripts

c	center
C	cap of Taylor bubble
d	diagonal
D	Danckwerts' method
F	liquid film
G	gas phase
L	liquid phase
TP	two-phase (gas + liquid)

References

[1] V. Hessel, P. Angelli, A. Gavriilidis, H. Lowe, *Ind. Eng. Chem. Res.* **2005**, *44*, 9750.

[2] T. Inoue, M. A. Schmidt, K. F. Jensen, *Ind. Eng. Chem. Res.* **2007**, *46*, 1153.

[3] K. Jahnisch, M. Baerns, V. Hessel, W. Ehrfeld, V. Haverkamp, H. Lowe, C. Wille, A. Guber, *J. Fluorine Chem.* **2000**, *105*, 117.

[4] N. de Mas, A. Gunther, M. A. Schmidt, K. F. Jensen, *Ind. Eng. Chem. Res.* **2003**, *42*, 698.

[5] R. D. Chambers, D. Holling, R. C. H. Spink, G. Sandford, G., *Lab Chip* **2001**, *1*, 132.

[6] K. K. Yeong, A. Gavriilidis, R. Zapf, V. Hessel, *Catal. Today* **2003**, *81*, 641.

[7] J. Kobayashi, Y. Mori, K. Okamoto, R. Akiyama, M. Ueno, T. Kitamori, S. Kobayashi, *Science* **2004**, *304*, 1305.

[8] R. Abdallah, P. Magnico, B. Fumey, C. de Bellefon, *AIChE J.* **2006**, *52*, 2230.

[9] R. Abdallah, V. Meille, J. Shaw, D. Wenn, C. de Bellefon, *Chem. Commun.* **2004**, *4*, 372.

[10] H. Ehrich, D. Linke, K. Morgenschweis, M. Baerns, K. Jahnisch, *Chimia* **2002**, *56*, 647.

[11] R. Gupta, D. F. Fletcher, B. S. Haynes, *J. Comp. Multiphase Flows* **2010**, *2*, 1.

[12] N. Shao, A. Gavriilidis, P. Angeli, *Chem. Eng. Sci.* **2009**, *64*, 2749.

[13] K. A. Triplett, S. M. Ghiaasiaan, S. I. Abdel-Khalic, D. L. Sadowski, *Int. J. Multiphase Flow* **1999**, *27*, 765.

[14] T. Cubaud, U. Ulmanella, C. M. Ho, *Fluid Dyn. Res.* **2006**, *38*, 772.

[15] S. Waelchli, P. R. von Rohr, *Int. J. Multiphase Flow* **2006**, *32*, 791.

[16] P. Sobieszuk, P. Cyganski, R. Pohorecki, *Chem. Eng. Res. Des.* **2010**, *88*, 236.

[17] A. Kawahara , P. M.-Y. Chung, M. Kawaji, *Int. J. Multiphase Flow* **2002**, *28*, 1411.

[18] I. Hassan, M. Vaillancourt, K. Pehlivan, *Microsc. Thermoph. Eng.* **2005**, *9*, 165.

[19] D. Liu, S. Wang, *Chem. Eng. Proc.* **2008,** *47, 2098.*

[20] M. K. Akbar, D. A. Plummer, S. M. Ghiaasiaan, *Int. J. Multiphase Flow* **2003**, *29*, 855.

[21] P. M. Y. Chung, M. Kawaji, *Int. J. Multiphase Flow* **2004**, *30*, 735.

[22] S. S. Y. Leung, Y. Liu, D. F. Fletcher, B. S. Haynes, *Chem. Eng. Sci.* **2010**, *65*, 6379.

[23] T. C. Thulasidas, M. A. Abraham, R. L. Cerro, *Chem. Eng. Sci.* **1995**, *50*, 183.

[24] S. Laborie, C. Cassabud, L. Durand-Bourlie, J. M. Laine, *Chem. Eng. Sci.* **1999**, *54*, 5723.

[25] M. T. Kreutzer, M. G. van der Eijnden, F. Kapteijn, J. A. Moulijn, J. J. Heiszwolf, *Catal. Today* **2005**, *105*, 667.

[26] H. Liu, C. O. Vandu, R. Krishna, *Ind. Eng. Chem. Res.* **2005**, *44*, 4884.

[27] M. K. Akbar, S. M. Ghiaansiaan, *Ind. Eng. Chem. Res.* **2006**, *45*, 5396.

[28] D. Qian, A. Lawal, *Chem. Eng. Sci.* **2006**, *61*, 7609.

[29] R. S. Abiev, *Theor. Found. Chem. Eng.* **2010**, *44*, 86.

[30] P. Garstecki, M. J. Fuerstman, H. A. Stone, G. M. Whitesides, *Lab Chip* **2006**, *6*, 437.

[31] V. van Steijn, C. R. Kleijn, M. T. Kreutzer, *Chem. Eng. Sci.* **2007**, *62*, 7505.

[32] V. van Steijn, C. R. Kleijn, M. T. Kreutzer, *Lab Chip* **2010**, *10*, 2513.

[33] M. de Menech, P. Garstecki, F. Jousse, H. A. Stone, *J. Fluid Mech.* **2008**, *595*, 141.

[34] N. Shao, W. Salman, A. Gavrirlidis, P. Angeli, *Int. J. Heat Fluid Flow* **2008**, *29*, 1603.

[35] R. Pohorecki, K. Kula, *Chem. Eng. Res. Des.* **2008**, *86*, 997.

[36] G. F. Christopher, N. N. Noharuddin, J. A. Taylor, S. L. Anna, *Phys. Rev. E* **2008**, *78*, 036317.

[37] J. H. Xu, S. W. Li, J. Tan, G. S. Luo, *Microfluid. Nanofluid.* **2008**, *5*, 711.

[38] T. Fu, Y. Ma, D. Funfschilling, C. Zhu, H. Z. Li, *Chem. Eng. Sci.* **2010**, *65*, 3739.

[39] F. Guo, B. Chen, *Microgravity Sci. Technol.* **2009**, *21*, 51.

[40] T. Abadie, J. Aubin, D. Legendre, C. Xuereb, *Microfluid. Nanofluid.* **2011**, *12*, 355.

[41] G. I. Taylor, *J. Fluid Mech.* **1961**, *10*, 161.

[42] T. C. Thulasidas, M. A. Abraham, R. L. Cerro, *Chem. Eng. Sci.* **1997**, *52*, 2947.

[43] A. Günther, S. A. Khan, M. Thalmann, F. Trachsel, K. F. Jensen, *Lab Chip* **2004**, *4*, 278.

[44] D. A. Fries, S. Waelchli, P. R. von Rohr, *Chem. Eng. J.* **2008**, *S135*, S37.

[45] P. Zaloha, J. Kristal, V. Jiricny, N. Völkel, C. Xuereb, J. Aubin, *Chem. Eng. Sci.* **2012**, *68*, 640.

[46] T. Taha, Z. F. Cui, *Chem. Eng. Sci.* **2004**, *59*, 1181.

[47] M. T. Kreutzer, F. Kapteijn, J. A. Moulijn, J. J. Heiszwolf, *Chem. Eng. Sci.* **2005,** *60, 5895.*

[48] K. Fukagata, N. Kasagi, P. Ua-arayaporn, T. Himeno, *Int. J. Heat Fluid Flow* **2007**, *28*, 72.

[49] D. A. Fries, S. P. R. von Rohr, *Chem. Eng. Sci.* **2009**, *64*, 1326.
[50] R. Gupta, D. F. Fletcher, B. S. Haynes, *Chem. Eng. Sci.* **2010**, *65*, 2094.
[51] J. Yue, G. Chen, Q. Yuan, L. Luo, Y. Gonthier, *Chem. Eng. Sci.* **2007**, *62*, 2096.
[52] P. Sobieszuk, P. Cyganski, R. Pohorecki, *Chem. Proc. Eng.* **2008**, *29*, 651.
[53] P. Sobieszuk, R. Pohorecki, P. Cyganski, J. Grzelka, *Chem. Eng. Sci.* **2011**, *66*, 6048.
[54] N. Völkel, *Ph. D. Thesis, Université de Toulouse* **2009.**
[55] W. B. Kolb, R. L. Cerro, *Chem. Eng. Sci.* **1991,** *46, 2181.*
[56] W. R. Dean, *Phil. Mag.* **1927**, *20*, 208.
[57] F. Trachsel, A. Günther, S. Khan, K. F. Jensen, *Chem. Eng. Sci.* **2005**, *60*, 5729.
[58] F. P. Bretherton, *J. Fluid. Mech.* **1961**, *12*, 2367.
[59] L. W. Schwartz, H. M. Princen, A. D. Kiss, *J. Fluid. Mech.* **1986**, *172*, 259.
[60] P. Aussillous, D. Quéré, *Phys. Fluids* **2000**, *12*, 2367.
[61] M. D. Giavedoni, F. A. Saita, *Phys. Fluids* **1997**, *9*, 2420.
[62] M. Heil, *Phys. Fluids* **2001**, *13*, 2517.
[63] Y. Han, N. Shikazano, *Int. J. Heat Fluid Flow* **2009**, *30*, 842.
[64] W. B. Kolb, R. L. Cerro, *Phys. Fluids A* **1993,** *5, 1549.*
[65] T. Taha, Z. F. Cui, *Chem. Eng. Sci.* **2006,** *61, 665.*
[66] Y. Han, N. Shikazano, *Int. J. Muliphase Flow* **2009**, *35*, 896.
[67] M. J. F. Warnier, E. V. Rebrov, M. H. J. M. De Croon, V. Hessel, J. C. Schouten, *Chem. Eng. J.* **2008,** *135S, S153.*
[68] J. Yun, Q. Lei, S. Zhang, A. Shen, K. Yao, *Chem. Eng. Sci.* **2010**, *65*, 5256.
[69] A. L. Hazel, M. Heil, *Chem. Eng. Sci.* **2002**, *470*, 91.
[70] A. Kuzmin, M. Januswewski, D. Eskin, F. Mostowfi, J. J. Dersken, *Chem. Eng. J.* **2011**, *178*, 306.
[71] D. M. Fries, F. Trachsel, P. R. von Rohr, *Int. J. Multiphase Flow* **2008**, *34*, 1108.
[72] R. W. Lockhart, R. C. Martinelli, *Chem. Eng. Prog.* **1949**, *45*, 39.
[73] D. Chisholm, *Int. J. Heat Mass Transfer* **1967**, *10*, 1767.
[74] K. Mishima, T. Hibiki, *Int. J. Multiphase Flow* **1996**, *22*, 703.
[75] H. J. Lee, S. Y. Lee, *Int. J. Multiphase Flow* **2001**, *27*, 783.
[76] S. Sairson, S. Wongwises, *Exp. Therm. Fluid Sci.* **2010**, *34*, 454.
[77] J. M. van Baten, R. Krishna, *Chem. Eng. Sci.* **2004**, *59*, 2535.
[78] R. Pohorecki, *Chem. Eng. Sci.* **2007**, *62*, 6495.
[79] G. Bercic, A. Pintar, *Chem. Eng. Sci.* **1997**, *52*, 3709.
[80] C. O. Vandu, H. Liu, R. Krishna, *Chem. Eng. Sci.* **2005**, *60*, 6430.
[81] J. Yue, L. Luo, Y. Gonthier, G. Chen, Q. Yuan, *Chem. Eng. Sci.* **2009**, *64*, 3697.
[82] J. M. van Baten, R. Krishna, *Chem. Eng. Sci.* **2005**, *60*, 1117.
[83] J. M. Commenge, T. Obein, G. Genin, X. Framboisier, S. Rode, V. Schanen, P. Pitiot, M. Matlosz, *Chem. Eng. Sci.* **2006**, *61*, 597.
[84] K. K. Yeong, A. Gavriilidis, R. Zapf, H. J. Kost, V. Hessel, A. Boyde, *Exp. Thermal Fluid Sci.* **2006**, *30*, 463.
[85] M. Al-Rawashdeh, V. Hessel, P. Löb, K. Mevissen, F. Schönfeld, *Chem. Eng. Sci.* **2008**, *63*, 5149.
[86] H. Zhang, G. Chen, J. Yue, Q. Yuan, *AIChE J.* **2009**, *55*, 1110.
[87] H. Monnier, N. Mhiri, L. Falk, *Chem. Eng. Proc.* **2010**, *49*, 953.
[88] J. M. Commenge, T. Obein, X. Framboisier, S. Rode, P. Pitiot, M. Matlosz, *Chem. Eng. Sci.* **2011**, *66*, 1212.
[89] P. Sobieszuk, R. Pohorecki, *Chem. Eng. Proc.* **2010**, *49*, 820.
[90] M. Zanfir, A. Gavriilidis, C. Wille, V. Hessel, *Ind. Eng. Chem. Res.* **2005**, *44*, 1742.
[91] P. Chasanis, A. Lautenschleger, E.Y. Kenig, *Chem. Eng. Sci.* **2010**, *65*, 1125.
[92] P. Sobieszuk, R. Pohorecki, P. Cyganski. M. Kraut, F. Olschewski, *Chem. Eng. J.* **2010**, *164*, 10.
[93] C. Horvath, B. A. Solomon, J. M. Engasser, *Ind. Eng. Chem. Fundam.* **1973**, *12*, 431.
[94] T. Obein, *Ph. D. Thesis*, Institut National Polytechnique de Lorraine, Nancy **2006**.
[95] K. Warmuzinski, J. Buzek, J. Podkanski, *Chem. Eng. J.* **1995**, *58*, 151.
[96] P. Angeli, A. Gavriilidis, *Proc. Inst. Mech. Eng. Part C: J. Mech. Eng. Sci.* **2008**, *222*, 737.
[97] G. Chen, J. Yue, Q. Yuan, *Chin. J. Chem. Eng.* **2008**, *16*, 663.
[98] M. N. Kashid, L. Kiwi-Minsker, *Ind. Eng. Chem. Res.* **2009**, *48*, 6465.
[99] A. A. Donaldson, A. Macchi, D. M. Kirpalani, *Chem. Eng. Sci.* **2011**, *66*, 3339.
[100] M. N. Kashid, A. Renken, L. Kiwi-Minsker, *Chem. Eng. Sci.* **2011**, *66*, 3876.
[101] S. Haase, T. Bauer, *Chem. Eng. J.* **2011**, *176–177*, 65.
[102] M. T. Kreutzer, F. Kapteijn, J. A. Moulijn, *AIChE J.* **2005**, *51*, 2428.
[103] R. Sun, T. Cubaud, *Lab Chip* **2011**, *11*, 2924.
[104] J. Tan, Y. C. Lu, J. H. Xu, G. S. Luo, *Chem. Eng. J.* **2012**, *181–182*, 229.
[105] D. Eskin, F. Mostowfi, *Int. J. Heat Fluid Flow* **2012**, *33*, 147.